# Size Effect of $CeO_2$ Particle On Nanoscale Single-Asperity Sliding Friction

**Ning Xu** ( xuning@sust.edu.cn )
Shaanxi University of Science and Technology Xi'an Campus: Shaanxi University of Science and Technology https://orcid.org/0000-0002-2883-1936
**Jiahui Ma**
Shaanxi University of Science and Technology Xi'an Campus: Shaanxi University of Science and Technology
**Qi Liu**
Shaanxi University of Science and Technology Xi'an Campus: Shaanxi University of Science and Technology
**Weizhong Han**
Xian Jiaotong University: Xi'an Jiaotong University
**Zhiwei Shan**
Xian Jiaotong University: Xi'an Jiaotong University

**Research Article**

**Keywords:** Single asperity friction, Size effect, Coefficient of friction (COF), CeO2

**Posted Date:** August 18th, 2021

**DOI:** https://doi.org/10.21203/rs.3.rs-786076/v1



**Version of Record:** A version of this preprint was published at Tribology Letters on December 2nd, 2021. See the published version at https://doi.org/10.1007/s11249-021-01544-5.

# Abstract

The size of abrasive particle has a great impact on the fundamental friction behavior and mechanical properties of the abrasive during ultra-precision polishing performance. Here, the size effect of the tribological behavior and mechanical properties of $CeO_2$ single abrasive were studied. Experimental results show that the size effect plays a role on coefficient of friction (COF) of each regime in single-asperity sliding friction, especially in ploughing and cutting regimes. The residual depth of the scratch and COF both decrease with the increase of the $CeO_2$ tip radius. These results relate to the mechanical properties of $CeO_2$ nanoparticles. We found that the effective modulus increases with the decrease of abrasive size, which corresponds to the size effect of the single-asperity sliding friction experiment.


# Introduction

The particle size of the abrasive has an obvious effect on the friction behavior and wear characteristics in two-body and three-body abrasive wear [1–10]. The study of size effect of abrasive in friction will be not only benefit for tribology innovation, but also referenced by the industry. For example, chemical mechanical polishing (CMP) is an important step in semiconductor manufacturing, where the size of the abrasive in the slurry can significantly affect the material removal rate (MRR) [11]. Zhou et al. [12, 13] studied the polishing properties of silicon oxide abrasives at 10 nm and 100 nm on silicon carbide and sapphire wafers, respectively, and found that large particle size was more beneficial to the MRR of silicon carbide wafers. However, when sapphire was polished, particle size had little effect on MRR, but small particles formed a lower surface roughness. At the same time, it also pointed out that the mechanical properties of abrasives can affect the polishing results. And Shen et al. [14] investigated the impact between coefficient of friction (COF) and material removal threshold. It is clear that the abrasive size has a significant influence on the predominant wear mechanisms, but there is no consensus on the effect of abrasives size on the wear process and mechanical properties of abrasive particles, especially at the micro-nano scale. Up to now, only a few researchers had been performed on the tribology mechanism of single abrasive wear at the micro-scale [15–19], which hinders the research progress of the abrasive size effect on friction behavior and the abrasive mechanical properties insufficient. The influence of abrasives size on the abrasive friction behavior and mechanical properties have attracted broad research interests [6, 7, 15]. The abrasive wear by performing single-asperity scratch with AFM silicon dioxide or tungsten tips were performed to study the influence of the abrasive size on the abrasive wear at the micro-scale [2]. It was found that the smaller tip radius causes more wear damage. Zhang et al. [7] used an AFM to discuss the nano-abrasion of the hydrogen-terminated silicon surface in water with spherical $SiO_2$ tips. It was found that the radius of the tip would seriously affect the removal of silicon surface material, and the large radius of the tip would cause a lot of wear and high friction. Chen et al. [20] found that small-size particles helped improve surface roughness after polishing experiments, and both small-size and large-size particles could achieve higher removal rate. An et al. [21] inferred that under normal circumstances, as the size decreases, NPA (Nanoparticle Abrasive) became harder and tougher. In addition to experimental research, both theoretic analysis and molecular dynamic simulations [22, 23]

were also employed to explore the relationship between the coefficient of friction and tip radius. In general, smaller particles not only improve the mechanical properties of the abrasive particles [24] and increase the effective contact area, but also increase the number of effective particles during the polishing, which is critical in elevating the MRR [25–27].

However, a macroscopic research of CMP usually assumes that each abrasive particle will produce the same effect, but in the actual CMP process, the size of the abrasive particle and the force of each particle on the wafer surface are vary randomly. The mechanical properties and friction behavior are usually affected by the chemical environment. During two-body wear, it is difficult to capture the actual size effect of a single abrasive particle and its deformation process at the micro-scale. However, studying the effect of abrasive size on atomic scale removal of silicon surface material can help reveal the microscopic removal mechanism of CMP [7]. A general cognition of wear performance can also help control the degree of wear and provide theoretical reference for ultra-precision surface machining and low damage defect production [28]. At the same time, since material removal is closely related to the mechanical properties of the abrasive particle, it is also necessary to discuss the influence of abrasive particle size on mechanical properties. In this study, through the nanoscratch method, the basic mechanism of single abrasive wear was realized by combining the homemade $CeO_2$ tips with different radii with the TriboIndenter system (TI 950) and the 2D transducer. Then, the Hysitron PicoIndenter85 (PI85) test system was used to mechanically test $CeO_2$ abrasive particles of different sizes in commercial polishing slurry, which proved that the size effect of the abrasives can significantly affect the actual mechanical properties of the abrasive particles.

## Experimental Section

# 2.1 Nanoscratch experiment of $CeO_2$ tips

The experimental setup of nanoscratch is displayed in Fig. 1(a). Using TI 950 in a humid environment and a dry atmosphere with a humidity of less than 5% (drying with silica gel desiccant for 12 h) for scratching behavior experiments, more accurate displacement and mechanical data can be obtained in two dimensions (normal and lateral). In this test, a 1.5 μm thick copper and TEOS ($SiO_2$) film was deposited on a commercial silicon wafer. The load function of the nanoscratch experiment can be divided into ramp and constant mode, as shown in Fig. 1(b). The ramp mode refers to the change of the normal force from point 0 to a preset point over time (such as 300 μN in Fig. 1(b)), while the constant mode means that normal force remains constant (such as 150 μN in Fig. 1(b)) during the scratch process. And the $CeO_2$ abrasive is used as a model system due to its high removal rate [29] and superior selectivity, which is widely used in the CMP industry [30, 31]. In order to prepare the nano-sized $CeO_2$ tips, a bulk sample of $CeO_2$ ceramic was prepared by sintering the $CeO_2$ nanoparticle synthesized by the hydrothermal method. The grain size of $CeO_2$ ceramics is in the range of 2 ~ 3 μm, which is big enough for milling single crystalline nano-sized tips. Then $CeO_2$ ceramic samples processed into curvature for ~ 30 μm is similar to the shape of needle tip (Fig. 1(c)) by a focused ion beam (FIB). The dark hole in the tip

body is the porosity of the $CeO_2$ ceramic. Finally, the nano-sized $CeO_2$ tip with a rectangular pyramid and cone angle of 60° was made by milling the tip of the needle $CeO_2$ rod using FIB with a fine beam. For more details, see our earlier work [32]. The SEM photos of the partial enlarged area of single side of the rectangular pyramid $CeO_2$ tip with different tip radii are shown in Figs. 1(d) to 1(f). The tip can be considered as a spherical-like rigid particle represented as the white dashed circles due to the scratch depth much less than the equivalent radius of the tip and the high hardness ratio of the $CeO_2$ to copper in this work. And the radius of homemade $CeO_2$ tips were calculated as 120 nm, 180 nm, and 270 nm, which are similar to abrasive particles used in the CMP industry [33]. And the nanoscratch length and scratch speed in the experiment were set as 8 μm and 0.5 μm/s, respectively. More details can be found in our previous work [32]. In order to decrease the experimental errors, we repeated the experiment 5 times on all the data. Under the well-controlled situation, the friction force, scratch depth, residue depth after the scratch step, the COF during the nanoscratch test can be measured. Here the residue depth refers to the depth left in the copper film after the nanoscratch test. And the COF represents for the ratio of the normal and lateral forces.

## 2.2 Mechanical performance of commercial $CeO_2$ abrasives

In order to test the mechanical properties of $CeO_2$ nanoparticles, it was necessary to separate the abrasive from the polishing slurry (Anjimirco Shanghai Co., Ltd., China). To separate the organic solvents, the polishing slurry was centrifuged and cleaned with alcohol, and then the pure $CeO_2$ particles were ultrasonically dispersed in ethanol so that the $CeO_2$ particles could be separately dispersed on a clean single crystal silicon wafer. The morphology of $CeO_2$ particles was examined by using a JEM-2100F high resolution transmission electron microscope (HR-TEM). Figure 2 is a schematic diagram of the nanomechanical test of $CeO_2$ particles and the nanocompressed morphology of commercially available $CeO_2$ particles. Figure 2(a) is an experimental schematic diagram of the PI85 test system for mechanical testing of $CeO_2$ particles adsorbed on the surface of monocrystalline silicon, and Fig. 2(b) shows a schematic diagram of the relationship between the $CeO_2$ particles dispersed on a single crystal silicon wafer and the diamond indenter system during the nanocompression experiment. We used TEM to perform imaging and diffraction analysis of the $CeO_2$ particles. The inset in Fig. 2(b) is the TEM image of commercial $CeO_2$ particles and their diffraction spots, showing that $CeO_2$ particles are almost spherical particles and single crystal nanoparticles. To make the compressed data easier to understand and calculate, we equated it to a sphere and assumed that the diameter of the sphere is the diameter of the circumscribed circle of the largest cross-section perpendicular to the compression direction (Fig. 2(b)). Therefore, according to the Hertz contact model, the relationship between the stress and strain of the particle during compression can be calculated. The stress at this time is defined as the area of the circumscribed circle of the largest cross-section, and the strain is defined as the amount of compression. And Fig. 2(c)-(d) shows the morphology before and after nanocompression. It is shown that nanoparticles undergo severe plastic deformation during the positive nanocompression process.

## Results And Discussions

# 3.1 Nano-scratch behavior of the $CeO_2$ tip on copper film

The residue depth as a function relation of the force with different radius of $CeO_2$ tips scratching on copper film with constant mode is shown in Fig. 3(a). We can see that the residue depth increased with the increase of the normal force for all cases in this work. The curves rise slowly when the normal force below 20 μN (within in the elastic stage) and then linear increase when the normal force after that. This variation trend of the residue depth comfortably with our early work [32] and the residue depth is near zero in the elastic regime and near linearly increase of residue depth during the changing elastic-plastic regime and steady elastic-plastic regime. Furthermore, there is an obvious size effect of the residue depth curve after the normal force of 20 μN. And then this size effect becomes more and more obvious with the increasing of the normal force. The residue depth decreased with the increase of the tip radius under the same normal force. That is the smaller particle size of the $CeO_2$ abrasive resulted in a greater scratch depth in the copper film under the same normal load. From the previous work [32], we know that the microscopic deformation of the copper surface transformed from the pure elastic, the variable elastic-plastic stages and pure plastic deformation as increasing the normal force during the nanoscratch process. Therefore, in the same situation, after the scratch test, the smaller the particle size, the greater the residual depth, which leads to the more serious plastic deformation of the copper surface. This can be attributed to the fact that smaller particles will cause higher compressive stress in the substrate under the same normal force. As we know, the removal rate of the chemical mechanical polishing almost in proportion to the normal force as reported by Cook in 1990 [34]. The experimental results demonstrate that in the micro-nano-scale wear process, under the same normal force, smaller abrasive particles can achieve higher removal rates.

At the same time, the variation of COF calculated with different tip radii on the normal force of copper film under the constant mode is shown in Fig. 3(b). It can be clearly seen that COF has a functional relationship with the change of normal force, and it can be divided into three stages, which are the adhesion, the ploughing, and the cutting regime as we reported previously [32]. Obviously, in the first regime, the three COF curves almost overlap each other. However, we should note that the first critical point of the COF curve doesn’t across at one normal force. The black, red, and blue solid points indicate the first critical point of the COF curves of the tip radius of 120 nm, 180 nm, and 270 nm as marked in Fig. 3(b), respectively. And we found that this trend also appeared at the second critical point of the COF curves, which is marked by the black, red, and blue hollow circles. And as shown in the hatched section in Fig. 3(b), we can see that the transformation of the critical point from the adhesion to the ploughing friction and from the ploughing to the cutting friction regime shift to the higher normal force with the increase of the tip radius. That is the size effect appears at the end of the adhesion regime and gets more significant after the adhesion regime and stable in the cutting regime in the COF plot. The COF has the potential to down with increasing of the tip radius.

In the previous study [32], two formulas in terms of the COF obtained via theory calculation and confirmed by our experimental data well. In the adhesion and ploughing regimes, the COF can be expressed by Eqs. (1) and (2), respectively.

$$COF = \frac{\pi}{K^{2/3}} \tau_a r^{2/3} N^{-1/3} \quad (1)$$

$$COF = \frac{\tau_p}{\sigma_p} \frac{4}{3\pi} \sqrt{\frac{2h}{r} - \left(\frac{h}{r}\right)^2} \quad (2)$$

where $\tau_a$, $\tau_p$ and $\sigma_p$ are the shear stress of in the adhesion regime, the shear stress and the yield stress of the ploughing regime, $r$ and $h$ are the tip radius and the scratch depth, the $N$ is the normal force and the $K$ is a constant that depends on Poisson's ratio and Young's model of the object material.

As we can see from Eq. (1), the *COF* goes to infinity by making the normal force (*N*) in the infinitely small. In the adhesion regime, the normal force slowly increases from zero and has a great impact on the *COF*, i.e. the particle size (*r*) seems to have no effect on the *COF* in this regime. That is the reason why there is no significant size effect in the first regime, which is consistent with the experimental results as shown in the overlap of the COF curve in Fig. 3(b). And the relationship between the *COF* and particle size (*r*) can be expressed by Eq. (2) when the nanoscratch moving into the second regime (the ploughing regime). From the experimental results, the COF strongly depends on the particle radius (*r*) during the ploughing regime in the nanoscrath. And we can see that the COF decreases with increasing the particle size when the scratch depth (*h*) less than the particle radius (*r*) and increases with increasing the particle size when the scratch depth (*h*) greater than the particle radius (*r*) by theoretical analysis of the Eq. (2). The scratch depth less than the tip radius used in this work, therefore the experimental results show that the COF decreases with the increase of the particle size in the ploughing regime as expected, i.e. the Eq. (2) obtained from theoretical simulation is only suitable for the case of the scratch depth less than the particle radius and no longer adaptable when the scratch depth increase further. When the nanoscratch goes into the last regime (the cutting regime), the COF is also influenced by the particle radius, but not by the normal force. And the COF in the cutting regime also shows the character of size effect and decreases with the increase of the particle radius.

## 3.2 Scratches on the TEOS film with $CeO_2$ tips

In order to confirm that the observed size effect of the COF is a general phenomenon rather than an accidental phenomenon, we conducted the nanoscratch experiment with a homemade $CeO_2$ tip on the TEOS film. We know the hardness of the $CeO_2$ tip and TEOS film are 7.35 GPa and 6.0 GPa as measured by TI 950. However, because the hardness of the tip is similar to that of the $SiO_2$ film, the $CeO_2$ tip is no longer suitable for use as a rigid particle in this system, i.e. the $CeO_2$ tip will inevitably be worn when scratched on the TEOS film. That is the size of the $CeO_2$ tip radius will become lager and lager with the progress of the nanoscratch procedure. However, that is good news for us, since the size of the tip radius can be regarded as increasing continuously in the nanoscratch test. As shown in Fig. 4, COF is a function of the normal force with $CeO_2$ tip scratches the silicon dioxide film under the ramp mode. The $CeO_2$ tip

was worn after the nanoscratch test, and the morphology before and after the wear is shown in Fig. 4. It is considered that there are four different sizes of tips (160 nm, *x* nm, *y* nm, and 1000 nm, 160 nm < *x* < *y* < 1000 nm) scratched the TEOS film in turns under the ramp mode, respectively. As shown in Fig. 4, the three friction regimes between the four curves of TEOS film and the COF curve on copper film are in good agreement. We can see that as the tip radius increases, the critical point between the three regimes, especially the critical point between the ploughing and cutting regime, shifts to a higher normal force. An obvious size effect of the COF appears at the beginning of the ploughing regime. At the same time, the ploughing regime (between the first and second critical points) expanded with increasing the tip radius. As shown in Fig. 4, for the tip radius of 160 nm, the second critical point is 350 μN, and for the 1000 nm, the second critical point is2 500 μN. And when the tip radius increases from 160 to 1000 nm, the range of the ploughing regime expands from 250 to 2250 μN.

From our previous work [32], we pointed out that the ploughing regime is a key stage to CMP due to the tunable material removal rate and the gentle scratching. From this work, we can conclude that by increasing the size of abrasive particles within the restricted range, the range in which the normal force affects the material removal efficiency can be expanded. In the past few decades, many scholars have studied the response of COF to the material removal rate by the in-situ CMP process monitor [35, 36], and there is a good correlation between COF and material removal rate. It can be concluded that the removal rate of CMP could be controlled by adjusting the COF between the abrasive and wafer. And we can adjust the COF by adjusting the size of the abrasive particles and the normal force of the nano-scratch experiment.

## 3.3 Mechanical properties of $CeO_2$ abrasives

We believe that the size effect of abrasive mechanical properties could be related to the results of nanoscratch experiments. Therefore, the mechanical performance of abrasives were tested using the displacement control method of the PI85 test system, i.e. the displacement of the indenter during the in-situ compression experiment was set to half of the particle's equivalent diameter, and then the abrasive was loaded and unloaded to obtain the corresponding loading and unloading curves. Figure 5 shows the positive force-compression displacement curves of $CeO_2$ particles with particle sizes of 80.8 nm, 90.0 nm, and 94.6 nm during the nanoindentation process. When the compression depth is about 10 nm, these three curves basically coincide. At this time, the particle size has no effect on the mechanical curve. And when the indentation depth further increases, the curve begins to diverge, showing a certain size effect, and this tendency becomes more and more obvious as the compression progresses. Finally, after unloading, all three particles have some degree of plastic deformation. The slope of the force-displacement curve shows a downward trend as the particle size increases, meaning that as the abrasive size decreases, the force required during compression also increases. By calculating the slope of the unloading section of the effective stress-strain curve, we can obtain the effective modulus of the particles. Figure 6 shows the effective stress-strain curve for particles with an equivalent diameter of 80.8 nm. The black line segment in the figure is obtained by fitting the unloading section of the curve, and the slope of the black line segment is the effective modulus of the particle. For the particle sizes of 80.0 nm,

90.0 nm, and 94.6 nm, the effective modulus of particles are 68.71 GPa, 56.11 GPa, and 54.67 GPa, respectively. The mechanical properties of nanoparticles exhibit a certain size effect and follow the "The smaller the stronger" principle [36].

The experimental results show that the size effect does exist and affects the mechanical properties of the abrasive, which will guide the improvement of the material removal rate.

# Conclusion

In this work, the tribology character of nanoscale between the single-asperity and a flat surface was used to study the mechanical process of $CeO_2$ abrasive particles in the CMP by our original method, and the mechanical properties of $CeO_2$ nanoparticles were tested by using in-situ compression experiments. The results show that the residual depth of scratches and COF both decreases with the increase of the $CeO_2$ tip radius. In particular, the size effect appears at the end of the adhesion regime and gets more significant after the adhesion regime and stable in the cutting regime. The experimental results also indicate that reducing the size of particle radius helps to improve the removal rate during nanowear, but it might narrow the choice of the normal force due to the narrowing of ploughing regime, which may be related to the mechanical properties of the particles. It is concluded that smaller particles have a larger effective modulus, reflecting that the mechanical properties of abrasive particles are also affected by size effect. This is a study of the effect of particle size on tribological behavior and mechanical properties. Many other factors (e.g. the moving speed of the abrasive [37], the chemical condition) may affect the result of CMP, and our next research direction will focus on these aspects.

# Declarations

## Funding

This work was financially supported by the National Nature Science Foundation of China (Nos. 51905324), the Scientific Research Program Funded by Shaanxi Provincial Education Department (Program No. 20JK0545), and the Doctoral Scientific Research Startup Foundation of Shaanxi University of Science and Technology (No. 2018BJ-14).

## Conflicts of interest/Competing interests

The authors declare that they have no known competing financial interests or personal relationships that could have appeared to influence the work reported in this paper.

## Availability of data and material

All data reported in a graphical format can be requested from the corresponding author.

## Code availability

Softwares and libraries used in this study are open source. Specific codes can be requested from the corresponding author.

### Authors' contributions

**Ning Xu:** Funding acquisition, Methodology, Resources, Formal analysis. **Jiahui Ma:** Writing the paper, Formal analysis. **Qi Liu:** Writing the paper. **Weizhong Han:** Supervision. **Zhiwei Shan:** Supervision.

### Ethics approval

Not applicable.

### Consent to participate

We declare that this work was approved by all participants.

### Consent for publication

We hereby confirm that this manuscript is our original work and has not been published nor has it been submitted simultaneously elsewhere. We further confirm that all authors have checked the manuscript and have agreed to the submission.

## References


1. Wang, C.T., Gao, N., Gee, M.G., Wood, R.J.K., Langdon, T.G.: Effect of grain size on the micro-tribological behavior of pure titanium processed by high-pressure torsion. Wear. **280–281**, 28–35 (2012). https://doi.org/10.1016/j.wear.2012.01.012
2. Woldman, M., Van Der Heide, E., Tinga, T., Masen, M.A.: The influence of abrasive body dimensions on single asperity wear. Wear. **301**, 76–81 (2013). https://doi.org/10.1016/j.wear.2012.12.009
3. Li, B., Fang, L., Sun, K.: Variance of Particle Size: Another Monitor to Evaluate Abrasive Wear. Tribol Lett. **55**, 465–472 (2014). https://doi.org/10.1007/s11249-014-0375-3
4. Zambrano, O.A., Coronado, J.J., Rodríguez, S.A.: Tempering Temperature Effect on Sliding Wear at High Temperatures in Mottled Cast Iron. Tribol Lett. **57**, 1–11 (2015). https://doi.org/10.1007/s11249-014-0462-5
5. Shen, M.-X., Dong, F., Zhang, Z.-X., Meng, X.-K., Peng, X.-D.: Effect of abrasive size on friction and wear characteristics of nitrile butadiene rubber (NBR) in two-body abrasion. Tribol Int. **103**, 1–11 (2016). https://doi.org/10.1016/j.triboint.2016.06.025
6. Kaushik, N.C., Rao, R.N.: Effect of grit size on two body abrasive wear of Al 6082 hybrid composites produced by stir casting method. Tribol Int. **102**, 52–60 (2016). https://doi.org/10.1016/j.triboint.2016.05.015
7. Zhang, P., He, H., Chen, C., Xiao, C., Chen, L., Qian, L.: Effect of abrasive particle size on tribochemical wear of monocrystalline silicon. Tribol Int. **109**, 222–228 (2017).

https://doi.org/10.1016/j.triboint.2016.12.050

8. Guo, X., Song, K., Liang, S., Wang, X., Zhang, Y.: Effect of Al2O3Particle Size on Electrical Wear Performance of Al2O3/Cu Composites. Tribol. Trans. **59**, 170–177 (2016). https://doi.org/10.1080/10402004.2015.1061079
9. Qin, K., Zhou, Q., Zhang, K., Feng, Y., Zhang, T., Zheng, G., et al.: Non-uniform abrasive particle size effects on friction characteristics of FKM O-ring seals under three-body abrasion. Tribol Int. **136**, 216–223 (2019). https://doi.org/10.1016/j.triboint.2019.03.051
10. Shen, M., Li, B., Zhang, Z., Zhao, L., Xiong, G.: Abrasive wear behavior of PTFE for seal applications under abrasive-atmosphere sliding condition. Friction. **8**, 755–767 (2019). https://doi.org/10.1007/s40544-019-0301-7
11. Jianxiu, S., Rui, X., Yipu, W., Jiejing, L., Haixu, L.: Study on Lapping Paste of 6H–SiC Single-Crystal Substrate in Tribochemical Mechanical Lapping. J Inst Eng (India): Ser E 21 (2020). https://doi.org/10.1007/s40034-020-00167-0
12. Zhou, Y., Pan, G., Gong, H., Shi, X., Zou, C.: Characterization of sapphire chemical mechanical polishing performances using silica with different sizes and their removal mechanisms. Colloids Surf, A. **513**, 153–159 (2017). https://doi.org/10.1016/j.colsurfa.2016.09.049
13. Zhou, Y., Pan, G., Shi, X., Xu, L., Zou, C., Gong, H., et al.: XPS, UV–vis spectroscopy and AFM studies on removal mechanisms of Si-face SiC wafer chemical mechanical polishing (CMP). Appl Surf Sci. **316**, 643–648 (2014). https://doi.org/10.1016/j.apsusc.2014.08.011
14. Shen, M., Li, B., Ji, D., Xiong, G., Zhao, L., Zhang, J., et al.: Effect of Particle Size on Tribological Properties of Rubber/Steel Seal Pairs Under Contaminated Water Lubrication Conditions. Tribol Lett 68 (2020). https://doi.org/10.1007/s11249-020-1285-1
15. Huang, P.Y.: A Material Removal Rate Model Considering Interfacial Micro-Contact Wear Behavior for Chemical Mechanical Polishing. J Tribol. **127**, 190–197 (2005). https://doi.org/10.1115/1.1828068
16. Liu, J., Notbohm, J.K., Carpick, R.W., Turner, K.T.: Method for characterizing nanoscale wear of atomic force microscope tips. Acs Nano. **4**, 3763 (2010). https://doi.org/10.1021/nn100246g
17. Vakarelski, I.U., Higashitani, K.: Single-Nanoparticle-Terminated Tips for Scanning Probe Microscopy. Langmuir. **22**, 2931–2934 (2006). https://doi.org/10.1021/la0528145
18. Zhu, A., He, D., He, S., Luo, W.: Material removal mechanism of copper chemical mechanical polishing with different particle sizes based on quasi-continuum method. Friction. **5**, 99–107 (2017). https://doi.org/10.1007/s40544-017-0142-1
19. Ilie, F.: Investigation into layers formed by selective transfer CMP mechanisms with atomic force microscope. J. Nanopart. Res. **13**, 5519–5526 (2011). https://doi.org/10.1007/s11051-011-0540-7
20. Chen, Y., Zuo, C., Chen, A.: Core/shell structured sSiO2/mSiO2 composite particles: The effect of the core size on oxide chemical mechanical polishing. Adv Powder Technol. **29**, 18–26 (2017). https://doi.org/10.1016/j.apt.2017.09.020
21. An, L., Zhang, D., Zhang, L., Feng, G.: Effect of nanoparticle size on the mechanical properties of nanoparticle assemblies. Nanoscale. **11**, 9563–9573 (2019). https://doi.org/10.1039/c9nr01082c

22. Zhu, P., Hu, Y., Fang, F., Wang, H.: Multiscale simulations of nanoindentation and nanoscratch of single crystal copper. Appl Surf Sci. **258**, 4624–4631 (2012). https://doi.org/10.1016/j.apsusc.2012.01.041
23. Zhu, P., Hu, Y., Wang, H., Ma, T.: Study of effect of indenter shape in nanometric scratching process using molecular dynamics. Mater Sci Eng, A. **528**, 4522–4527 (2011). https://doi.org/10.1016/j.msea.2011.02.035
24. Rezaee-Hajidehi, M., Stupkiewicz, S.: Phase-field modeling of multivariant martensitic microstructures and size effects in nano-indentation. Mech. Mater. **141**, 103267 (2020). https://doi.org/10.1016/j.mechmat.2019.103267
25. Wang, Y., Zhao, Y., Li, X.: Modeling the effects of abrasive size, surface oxidizer concentration and binding energy on chemical mechanical polishing at molecular scale. Tribol Int. **41**, 202–210 (2008). https://doi.org/10.1016/j.triboint.2007.08.004
26. Wang, Y., Zhao, Y., An, W., Ni, Z., Wang, J.: Modeling effects of abrasive particle size and concentration on material removal at molecular scale in chemical mechanical polishing. Appl Surf Sci. **257**, 249–253 (2010). https://doi.org/10.1016/j.apsusc.2010.06.077
27. Zheng, M., Wang, B., Zhang, W., Cui, Y., Zhang, L., Zhao, S.: Analysis and prediction of surface wear resistance of ball-end milling topography. Surf Topogr: Metrol Prop 8 (2020). https://doi.org/10.1088/2051-672X/ab9d70
28. Yuan, S., Guo, X., Huang, J., Gou, Y., Jin, Z., Kang, R., et al.: Insight into the mechanism of low friction and wear during the chemical mechanical polishing process of diamond: A reactive molecular dynamics simulation. Tribol Int 148 (2020). https://doi.org/10.1016/j.triboint.2020.106308
29. Wang, Z.L., Dong, X.F.: Polyhedral shapes of CeO2 nanoparticles. J Phys Chem B. **107**, 13563–13566 (2003). https://doi.org/10.1021/jp036815m
30. Larsen-Basse, J., Liang, H.: Probable role of abrasion in chemo-mechanical polishing of tungsten. Wear s. **235**, 233 (1999). https://doi.org/10.1016/S0043-1648(99)00248-3.. –:647–654 ).
31. Castillo-Mejia, D., Beaudoin, S.A., Locally Relevant: Prestonian Model for Wafer Polishing. J Electrochem Soc 150:G96-G102 (2003). https://doi.org/10.1149/1.1532330
32. Xu, N., Han, W., Wang, Y., Li, J., Shan, Z.: Nanoscratching of copper surface by CeO2. Acta Mater. **124**, 343–350 (2017). https://doi.org/10.1016/j.actamat.2016.11.008
33. Chen, Y., Long, R.: Polishing behavior of PS/CeO2 hybrid microspheres with controlled shell thickness on silicon dioxide CMP. Appl Surf Sci. **257**, 8679–8685 (2011). https://doi.org/10.1016/j.apsusc.2011.05.047
34. Cook, L.M.: Chemical processes in glass polishing. J. Non-Cryst. Solids. **120**, 152–171 (1990). https://doi.org/10.1016/0022-3093(90)90200-6
35. Uchic, M.D., Shade, P.A., Dimiduk, D.M.: Plasticity of Micrometer-Scale Single Crystals in Compression. Annu. Rev. Mater. Sci. **39**, 361–386 (2009). https://doi.org/10.1146/annurev-matsci-082908-145422

36. Dehm, G.: Miniaturized single-crystalline fcc metals deformed in tension: New insights in size-dependent plasticity. Prog. Mater Sci. **54**, 664–688 (2009). https://doi.org/10.1016/j.pmatsci.2009.03.005

37. Zhu, J., Xiong, C., Ma, L., Zhou, Q., Huang, Y., Zhou, B., et al.: Coupled effect of scratching direction and speed on nano-scratching behavior of single crystalline copper. Tribol Int. **150**, 106385 (2020). https://doi.org/10.1016/j.triboint.2020.106385

# Figures

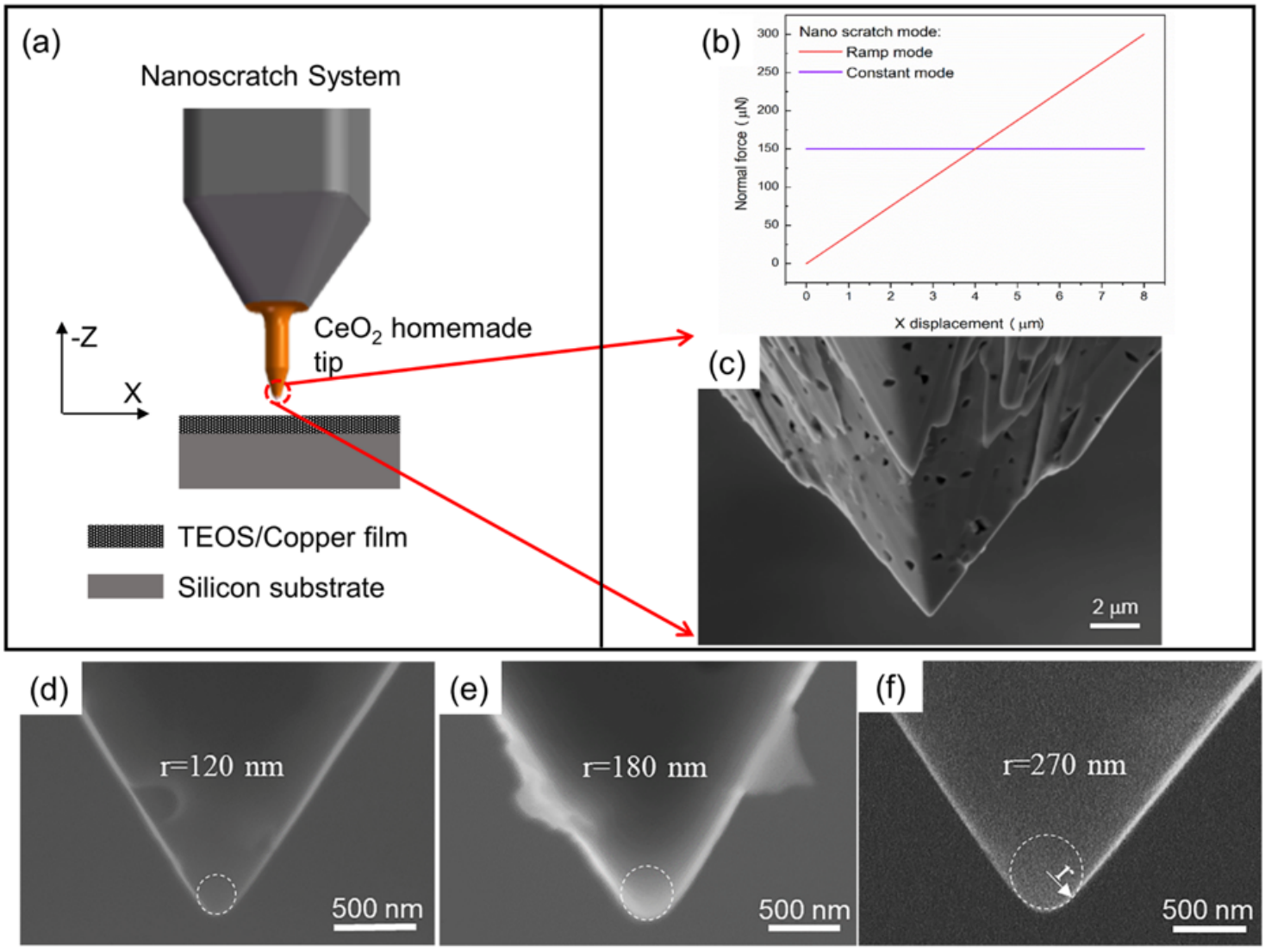


**Figure 1**

Schematic diagrams of nanoscratch system and SEM image of homemade CeO2 tips. (a) The setup of the nanoscratch experiment with the homemade CeO2 tip; (b) The load function of the two nanoscratch modes (constant mode and ramp mode); (c) The SEM image of the rectangular pyramid shape of the homemade CeO2 tip; (d)-(f) The typical SEM images of the front of the CeO2 tips with different tip radii.

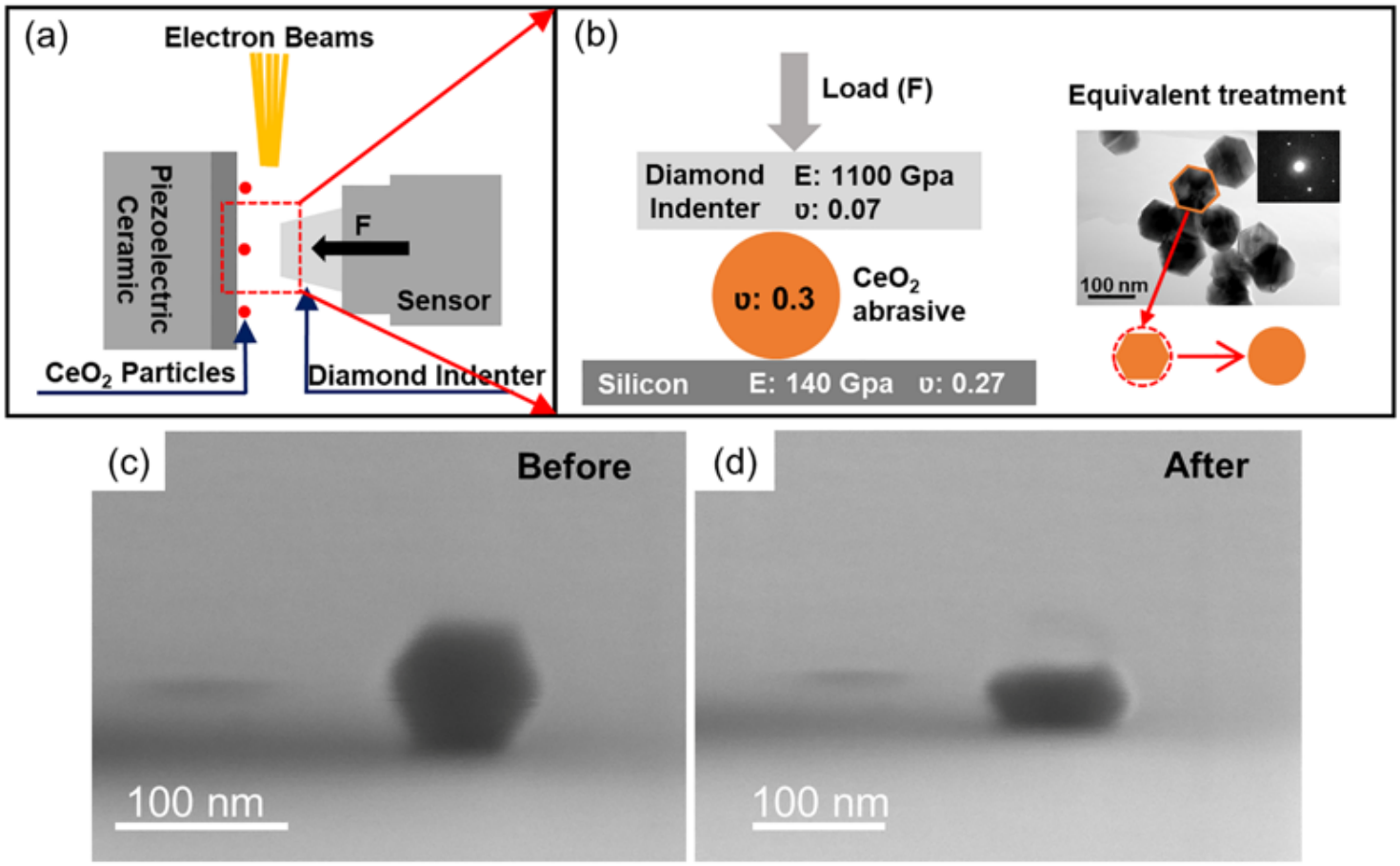


## Figure 2

Schematic diagrams of the nanomechanical testing system and the nanocompressed morphology of CeO2 particles. (a) Schematic diagram of the compression experiment of the PI85 system on CeO2 particles; (b) Schematic diagram of nanocompression of the equivalent CeO2 particle and TEM image of CeO2 particles; (c)-(d) CeO2 particles before and after the compression test.

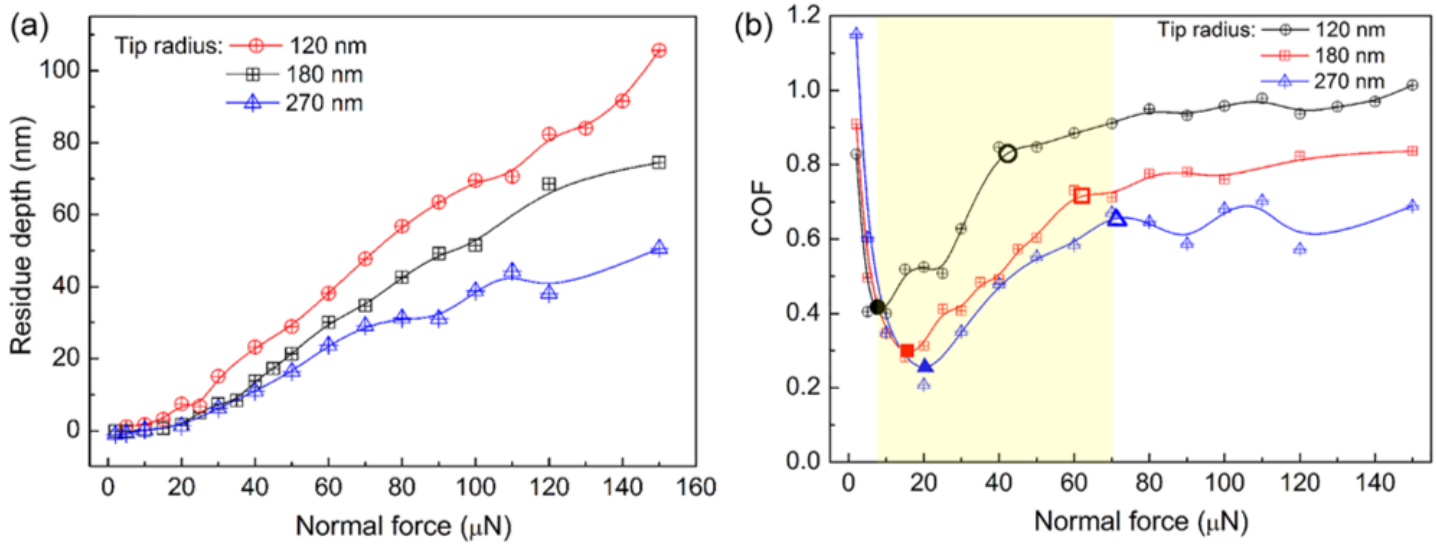


## Figure 3

The residue depth (a) and the coefficient of friction (b) measured during scratching on copper film as a function of normal force with different size (r=120 nm, 180 nm, 270 nm) of CeO2 tip under constant mode.

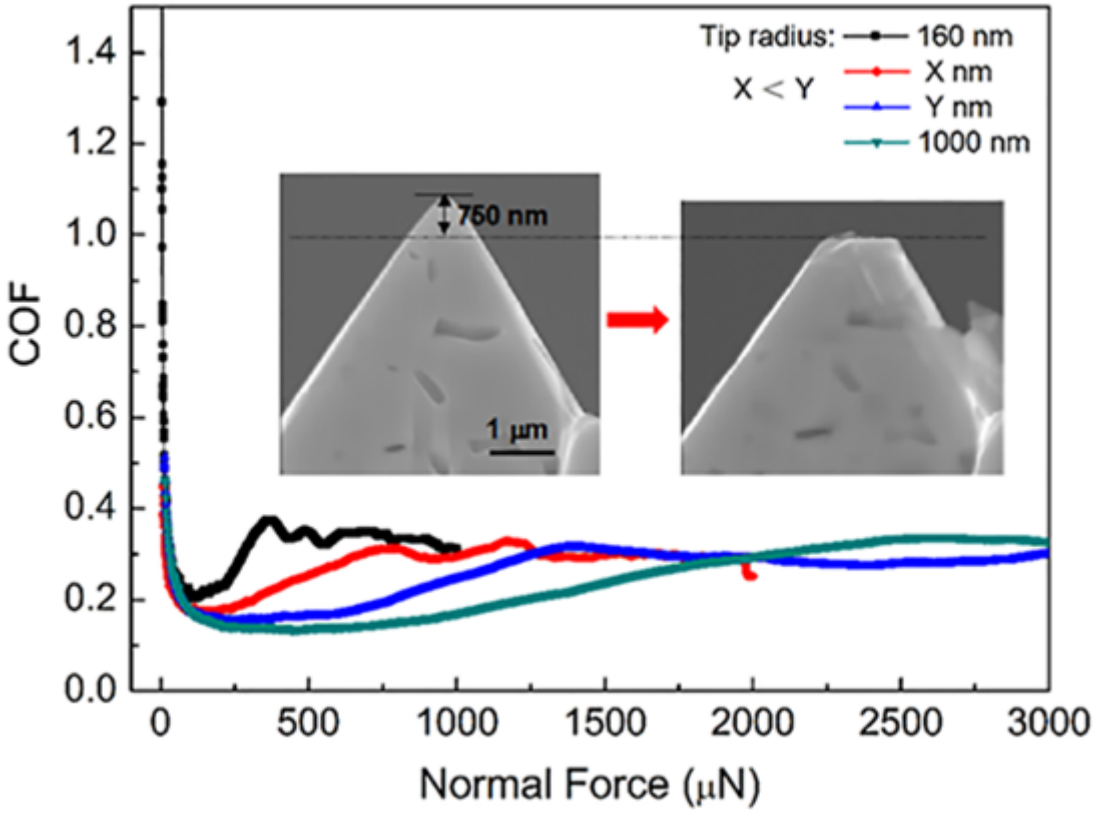


**Figure 4**

The coefficient of the friction force measured during scratching on silicon dioxide as a function of the normal force for different size of CeO2 tip under ramp force mode.

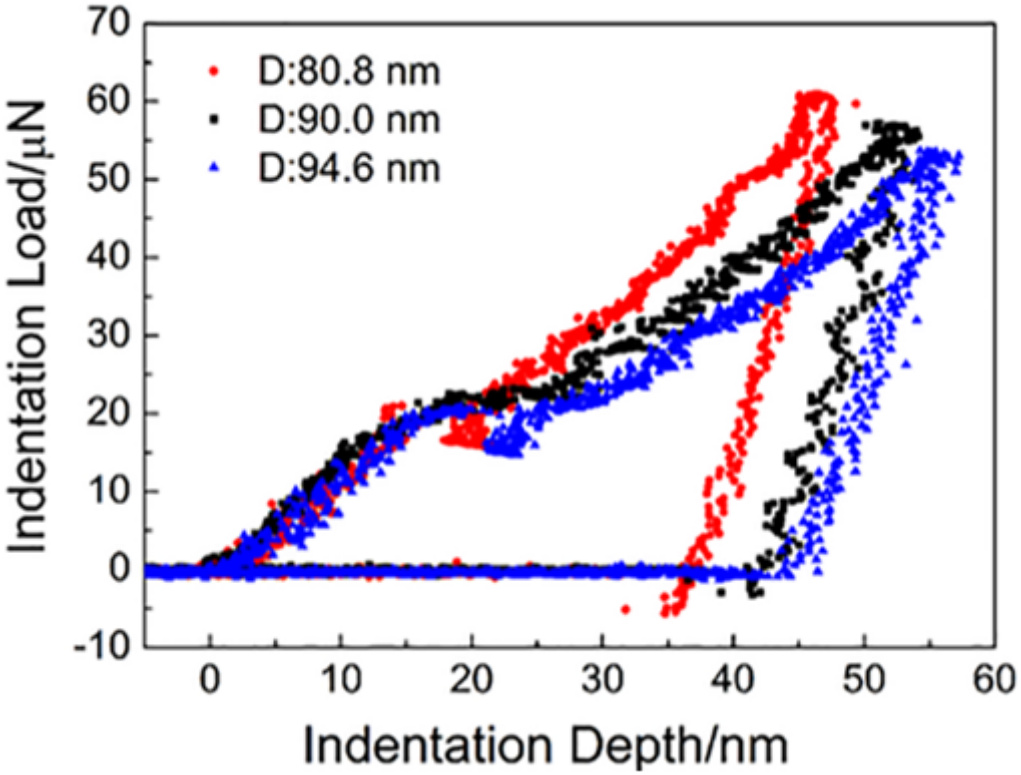


**Figure 5**

Compression force-compression displacement curves of cerium oxide nanoparticles with different particle sizes.

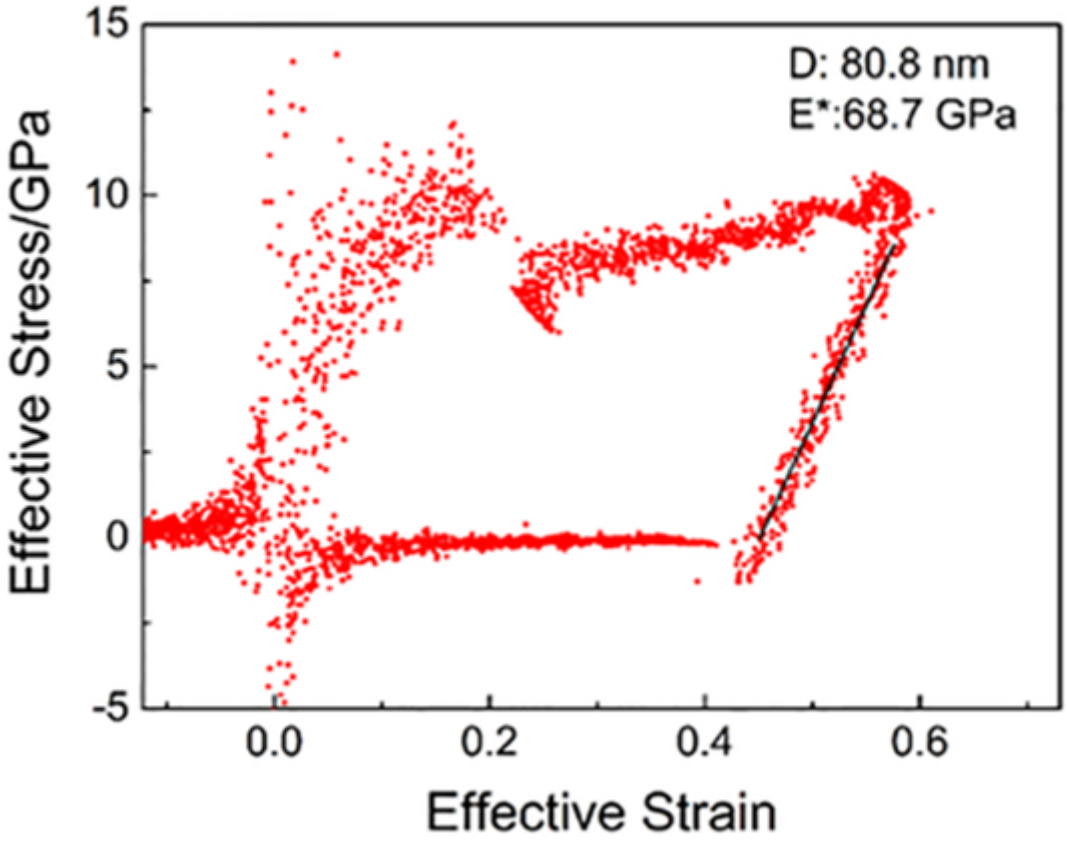


**Figure 6**

The effective stress-strain curve of CeO2 particles with an equivalent particle size of 80.8 nm.

## Supplementary Files

This is a list of supplementary files associated with this preprint. Click to download.

- GraphicalAbstract.tif